P-wave tomography of eastern North America: Evidence for mantle evolution from Archean to Phanerozoic, and modification during subsequent hot spot tectonism

M. Villemaire,[1] F. A. Darbyshire,[1] and I. D. Bastow[2]

Received 18 July 2012; revised 18 October 2012; accepted 18 October 2012; published 8 December 2012.

[1] The unique physical and chemical properties of cratonic lithosphere are thought to be key to its long-term survival and its resistance to pervasive modification by tectonic processes. Study of mantle structure in southeast Canada and the northeast US offers an excellent opportunity to address this issue because the region spans 3 billion years of Earth history, including Archean formation of the Superior craton and younger accretion of terranes to eastern Laurentia during the Proterozoic Grenville and Phanerozoic Appalachian orogenies. Trending NW–SE through each of these terranes is the track of the Great Meteor hot spot, which affected the region during the Mesozoic. Here we study mantle seismic velocity structure beneath this region of eastern North America using tomographic inversion of teleseismic P-wave relative arrival-times recorded by a large-aperture seismograph network. There are no large-scale systematic differences between Superior and Grenville mantle wave speed structure, which may suggest that tectonic stabilization of cratons occurred in a similar fashion during the Archean and Proterozoic. Cratonic lithosphere is largely thought to be resistant to modification by hot spot processes, in contrast to younger terranes where lithospheric erosion and significant magmatism are expected. Low velocities beneath the regions affected by the Great Meteor hot spot are broadest beneath the Paleozoic Appalachian terranes, indicating pervasive modification of the lithosphere during magmatism. The zone of modification narrows considerably into the Proterozoic Grenville province before disappearing completely in the Archean Superior craton, where the surface signature of Mesozoic magmatism is limited to kimberlite eruptions.

Citation: Villemaire, M., F. A. Darbyshire, and I. D. Bastow (2012), P-wave tomography of eastern North America: Evidence for mantle evolution from Archean to Phanerozoic, and modification during subsequent hot spot tectonism, *J. Geophys. Res.*, *117*, B12302, doi:10.1029/2012JB009639.

1. Introduction

[2] Shields are vast areas of Earth's surface that formed during the Precambrian. In seismic tomographic images most are easily identified by their high seismic wave speed roots, which can extend to depths of ≥250 km [e.g., *Lekic and Romanowicz*, 2011]. The processes responsible for shield formation are controversial, however, because there is no consensus on the timing of onset of Phanerozoic-style plate tectonics: it has been estimated to be as early as 4.1 Ga [e.g., *Hopkins et al.*, 2008], or as late as 1 Ga [e.g., *Stern*, 2005]. The reason for the shields' ability to resist thermal and mechanical erosion throughout multiple Wilson cycles is similarly not well understood, though an established factor is their intrinsically buoyant chemically-depleted lithospheric keel [e.g., *King*, 2005; *Lee et al.*, 2011]. The cratonic keels are generally associated with high lithospheric strength, relatively cold temperatures and high buoyancy, often assumed to reflect processes in a hotter Earth [e.g., *Jordan*, 1988]. Existing models for keel formation largely invoke Archean processes, such as the extraction of komatiitic magmas [e.g., *Griffin et al.*, 1999] to explain the intrinsic low density of the tectosphere.

[3] The cratonic lithosphere is highly depleted in basaltic components, with low concentrations of elements such as Al, Ca and Fe. This chemical depletion, in combination with the low temperatures, results in high seismic wave speeds in the cratonic keels, despite their relatively low density [e.g., *Jordan*, 1988; *King*, 2005; *O'Reilly and Griffin*, 2006]. These high seismic wave speeds have been used to identify and characterize cratons worldwide through tomographic imaging, though exact definitions of the keel thickness

[1]Centre de Recherche GEOTOP, Université du Québec à Montréal, Montreal, Quebec, Canada.
[2]Department of Earth Science and Engineering, Imperial College London, UK.

Corresponding author: F. A. Darbyshire, Centre de Recherche GEOTOP, Université du Québec à Montréal, CP 8888 Succursale Centre-Ville, Montréal, QC H3C 3P8, Canada. (darbyshire.fiona_ann@uqam.ca)

0148-0227/12/2012JB009639

(depth to the base of the lithosphere) with respect to the details of the seismic wave speed anomalies vary considerably [e.g., *Eaton et al.*, 2009].

[4] The largest continental keel on Earth is that beneath Laurentia, the cratonic core of North America, where the geological record spans more than 2 billion years of the Precambrian from the Archean formation of the Superior craton to the Proterozoic Grenville orogen [*Hoffman*, 1988]. After accretion of the Appalachian terranes to eastern Laurentia during the Paleozoic, no further significant episodes of magmatism or tectonism affected the region until the passage of the Great Meteor hot spot at ~200–110 Ma [e.g., *Heaman and Kjarsgaard*, 2000]. The hot spot track extends ~6000 km from northern Hudson Bay to the northeast US coast, and continues southeast as a chain of Atlantic seamounts. Eastern North America thus represents an excellent opportunity to address questions associated with Precambrian tectonics, and the ability of the lithosphere to resist modification by hot spot tectonism.

[5] While a wealth of seismic data has existed for several years from broadband seismograph stations in the northeast US and southern Canada, efforts to compare these regions to the Canadian Shield further north have been limited due to a lack of station coverage. In the early to mid 2000s, data coverage in eastern and northern Ontario was significantly improved through the POLARIS (Portable Observatories for Lithospheric Analysis and Research Investigating Seismicity [*Eaton et al.*, 2005]) project, but it was not until the latter half of the decade that a similar level of data coverage was achieved in central and southern Québec. The combined data set thus provides an ideal opportunity to study structural variations from the core of the Canadian Shield to the northern US continental margin, in order to provide new insight into past and present tectonic processes in eastern North America.

[6] Here we present a teleseismic P-wave relative arrival-time tomographic study of mantle seismic wave speed structure in eastern Laurentia using data from seismograph networks that span Archean, Proterozoic and Paleozoic terranes, each affected by the Great Meteor hot spot (Figure 1). Our results have important implications for the processes that formed and shaped the Canadian Shield during Precambrian times, and shed new light on the effects of intra-plate hot spot tectonism.

1.1. Tectonic Setting

[7] The largest craton on Earth, the Superior craton, formed in the late Archean from a collage of fragments of both continental and oceanic affinity [e.g., *Ludden and Hynes*, 2000; *Percival*, 2007]. Progressive southward younging of provinces within the craton suggest that it developed due to successive subduction and accretion [e.g., *Percival et al.*, 2006], culminating with the Kenoran orogeny at ~2.68 Ga. The oldest domain within the central-eastern Superior is the ~3 Ga Opatica province, comprising rocks of largely continental affinity. Domains further to the north (e.g., Opinaca, La Grande and Bienville) also show a continental ancestry. In contrast, one of the youngest domains, the Wawa—Abitibi subprovince (the largest area of greenstone belts worldwide), shows an oceanic affinity. The rocks within this region consist largely of volcanic and plutonic assemblages associated with ocean floor and arc settings. The Abitibi subprovince accreted to the Opatica domain at ~2.69 Ga. To the south, the smaller Pontiac domain is thought to be a fold-thrust belt overridden by the southern Abitibi [e.g., *Percival*, 2007].

[8] The Superior craton is bounded by Proterozoic orogenic belts. The main phase of assembly of Laurentia, the Trans-Hudson Orogen (THO), occurred in Paleoproterozoic times when the Superior plate collided with the Churchill plate (in present-day Hudson Bay) at ~1.8 Ga [*Hoffman*, 1988]. The THO is believed to have been an orogeny akin to the ongoing Himalayan-Karakoram-Tibetan orogen of Asia [e.g., *St.-Onge et al.*, 2006].

[9] Subsequent periods of accretion affected the southeast margin of the craton [e.g., *Whitmeyer and Karlstrom*, 2007], with a series of collisions of island arcs, back-arc terranes and continental fragments. This period culminated in the Grenvillian orogeny at ~1 Ga, associated with the formation of the supercontinent Rodinia. The present-day Grenville province is a complex region, comprising reworked rocks from the Laurentian margin and younger arc-related material. The Superior-Grenville boundary is also complex, with indications that Archean material underlies parts of the northern Grenville province [e.g., *Ludden and Hynes*, 2000], extending the Laurentian keel beneath both Archean and Proterozoic crust.

[10] Breakup of Rodinia along the southeastern margin of Laurentia began at ~620 Ma. There is evidence for the development of a network of failed rift arms of late Precambrian age in our study region [*Kamo et al.*, 1995], including the Ottawa-Bonnechere graben and its northwest extension, the Lake Timiskaming structural zone, prior to the opening of the Iapetus ocean (Figure 1). Closure of the Iapetus ocean and the development of the Appalachians [e.g., *Hatcher*, 2005; *van Staal*, 2005] took place over the period 462–265 Ma through a series of continent-arc and continent-continent collisions, culminating in the Laurussia—Gondwana collision that marked the assembly of the supercontinent Pangea. Rifting of Pangea at ~180 Ma initiated the separation of Laurussia and Gondwana, and the opening of the central North Atlantic ocean.

[11] Eastern Laurentia has been affected by magmatic processes likely associated with hot spots through much of its geologic history. Several large radiating dyke swarms dating from the periods throughout the Proterozoic are emplaced in the Superior and Grenville crust [e.g., *Ernst and Buchan*, 2001; *Ernst and Bleeker*, 2010]. There is also evidence from both epirogenic uplift and magmatism for the passage of a hot spot beneath North America in the Mesozoic [*Sleep*, 1990]. *Heaman and Kjarsgaard* [2000] correlated the age progression of kimberlites (~190–150 Ma), alkaline igneous intrusions and other magmatic activity (~130–100 Ma) along a northwest-southeast track beneath eastern Canada and the northeast US, continuing offshore with the New England seamount chain. The track of magmatic activity is postulated to represent the interaction of the Great Meteor hot spot with the North American lithosphere.

1.2. Previous Geophysical Studies

[12] Most regional-scale studies previously carried out in eastern Canada focused on the detailed structure of the continental crust and uppermost mantle, using data from reflection and refraction profiles. The Abitibi-Grenville

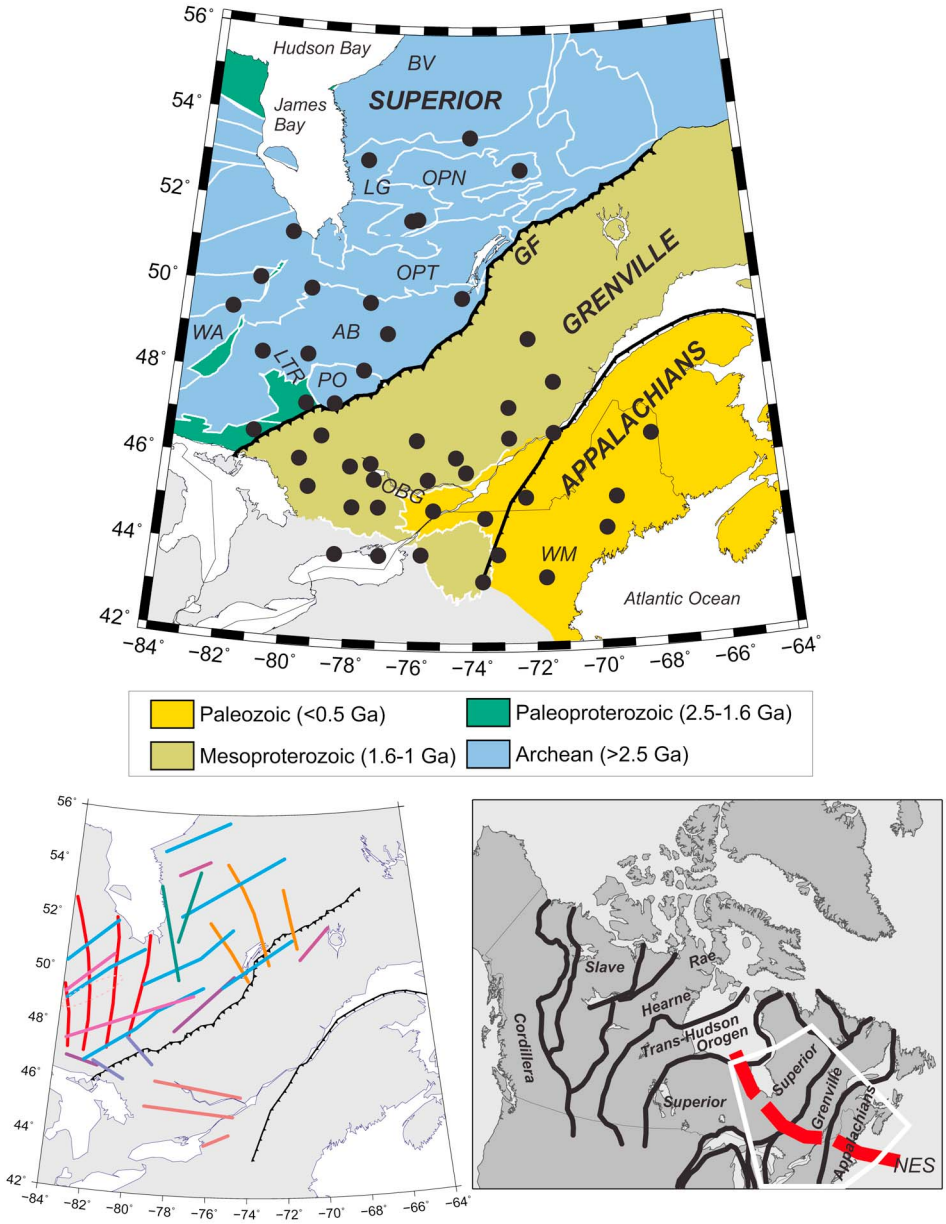

Figure 1. (top) Tectonic map of the southeastern Canadian Shield and northeastern Appalachian region. The tectonic boundaries in Canada are taken from digital compilations of maps produced through the Lithoprobe programme [*Clowes*, 2010]. Black circles show locations of seismograph stations; see Table 1 for network affiliations and sensor types. Tectonic divisions — AB: Abitibi, OPT: Opatica, OPN: Opinaca, LG: La Grande, BV: Bienville, WA: Wawa, PO: Pontiac, GF: Grenville Front [after *Percival*, 2007], NES: New England seamounts, WM: White Mountains, OBG: Ottawa-Bonnechere graben, LTR: Lake Timiskaming Rift. (bottom left) Map of the study area showing the locations of Proterozoic dike swarms that have affected the region, after *Ernst and Bleeker* [2010]. The dike swarms range in age from ~2.5 Ga to ~590 Ma and are grouped by color according to age. (bottom right) Map of Canada showing major terrane boundaries (black lines), the study area (white outline) and the inferred track of the Great Meteor hot spot [e.g., *Heaman and Kjarsgaard*, 2000].

(AG) transect of the Lithoprobe programme [e.g., *Clowes*, 2010] imaged crustal structure in our region of interest, in particular a north-south profile that crossed from the Grenville province into the Superior craton terranes. The seismic reflection images [*Calvert et al.*, 1995] showed a large-scale northward-dipping structure extending below the Moho; this was interpreted as a relict of accretion between the Abitibi and Opatica domains, possibly implying subduction-like processes operating in the Neoarchean. If this is the case, then the reflector would likely correspond to the top of a 'fossil' slab.

[13] A regional travel-time tomography study was carried out along the teleseismic component of the AG transect, which comprised a north-south linear array (ABI-96) of broadband seismographs [*Rondenay et al.*, 2000]. Due to the geometry of the array, the aperture of the resulting mantle model was limited, but the study identified a NW-SE trending low-velocity corridor in the top ~300 km of the mantle, with a steep dip and narrow width (~120 km). The anomaly was interpreted to represent upper-mantle modification arising from the passage of the Mesozoic Great Meteor hot spot, possibly localized along zones of lithospheric weakness caused by late Precambrian / early Paleozoic rifting, and caused by a combination of compositional and residual thermal effects. The travel-time tomography study of *Aktas and Eaton* [2006] in the Great Lakes region overlapped with the southern part of the ABI-96 array, and the models showed a patchy low-velocity anomaly trending roughly NW-SE in a similar location to that imaged by *Rondenay et al.* [2000]. This low-velocity feature continues to the southeast across New England, as imaged in body and surface wave regional tomographic models [*Levin et al.*, 1995; *Li et al.*, 2003]. A spatial correlation with regional magmatism and crustal seismicity was noted, and the authors suggested that the Mesozoic hot spot magmatism exploited pre-existing lateral heterogeneities and weaknesses in the continental lithosphere related to late-Precambrian Iapetan rifting events.

[14] In continental-scale tomographic models [e.g., *van der Lee and Frederiksen*, 2005; *Nettles and Dziewonski*, 2008; *Bedle and van der Lee*, 2009], seismic velocities associated with the Canadian Shield are significantly higher than the global average to depths of at least 200–250 km. This high-velocity 'lid' is interpreted as the seismic expression of the cold, depleted, buoyant cratonic lithosphere [e.g., *Eaton et al.*, 2009; *Fischer et al.*, 2010]. In contrast, the models show seismic velocities close to the global average for the mantle beneath the northeast US. The southeast corner of the lithosphere in the Great Lakes region contains a dent or 'divot', where normal-wave speed mantle intrudes into the high-velocity shield [e.g., *van der Lee and Frederiksen*, 2005; *Nettles and Dziewonski*, 2008; *Bedle and van der Lee*, 2009]. This feature correlates spatially with the southeastern extent of the low-velocity corridors imaged in the regional-scale studies, and is interpreted to represent lithospheric modification or erosion arising from the interaction of the hot spot with the lithospheric keel.

[15] The location of the 'divot' at depth, compared to surface features associated with the proposed Great Meteor hot spot track and with its reconstructed path, was studied by *Eaton and Frederiksen* [2007]. Low-velocity anomalies at 200 km depth appear to be offset from surface features such as kimberlites and other magmatism, and the degree of offset increases with age along the proposed hot spot track. The authors interpreted the misalignment as arising from deformation of the base of the lithosphere due to asthenospheric flow.

[16] Global-to-continental-scale tomographic models show that mid-mantle seismic structure beneath eastern North America is dominated by the presence of the subducting Farallon slab and the mantle wedge above it [e.g., *Grand et al.*, 1997; *van der Lee et al.*, 2008; *Li et al.*, 2008; *Sigloch*, 2011]. Some of these models also suggest smaller-scale high-velocity features above the Farallon slab.

[17] Our new tomographic model provides higher resolution over a larger array aperture than previous studies, due to the use of new seismograph networks. This allows for a more detailed image of the low-wave speed 'divot', in particular its magnitude and 3D geometry, and explores differences in lithospheric structure between Archean, Proterozoic and Phanerozoic mantle. The body-wave model also affords significantly higher lateral resolution than earlier surface wave studies.

2. Methodology

2.1. Seismograph Networks and Teleseismic Data Set

[18] This study utilizes teleseismic P-wave travel-time data from 47 seismograph stations centered on the Québec-Ontario region of eastern Canada (Figure 1). Canadian data from permanent seismograph stations (e.g., Canadian National Seismograph Network - CNSN) were supplemented by recordings from temporary POLARIS network installations, and a new deployment of stations by the Université du Québec à Montréal. The network aperture is ~1100 × 1100 km, with an average station spacing of ~100 km. Most stations in the network were equipped with broadband seismometers (Streckheisen STS-1 or STS-2, Güralp CMG-3ESP, CMG-3T or CMG-40T, or Nanometrics Trillium 120PA), except for 10 stations that use short-period sensors. Station and network details are given in Table 1. Instrument responses were standardized across the network prior to analysis.

[19] For the 27-month period spanning October 2007 to December 2009 when our stations were operating synchronously, we recorded 956 magnitude mb ≥5.5 earthquakes in the teleseismic distance range 30°–103°. Visual inspection of these recordings yielded a subset of 184 earthquakes (Figure 2) of sufficiently high signal-to-noise ratio for use in relative arrival-time analysis.

2.2. Method of Relative Arrival-Time Determination

[20] Manual picking of the first arriving P-wave identifiable across the network was performed on waveforms that were filtered with a zero-phase two-pole Butterworth filter with corner frequencies of 0.7–3 Hz. Filter bandwidths were designed to retain as high a frequency as possible since our inversion procedure adopts ray theory (the infinite frequency approximation). Our chosen bandwidths were similar to those used in other tomographic studies in both tectonically active settings (e.g., P, 0.8–2 Hz [*Allen et al.*, 2002]; 0.4–2 Hz [*Bastow et al.*, 2008]) and quieter shield areas (e.g., P, 0.4–2 Hz [*Sol et al.*, 2002]).

[21] After manual picking, phase arrivals were subsequently refined, and relative arrival-time residuals determined using the multichannel cross-correlation (MCCC) technique of *VanDecar and Crosson* [1990]. During the MCCC procedure, a 3 s window was selected for cross-correlation, containing the initial phase arrival and typically one or two cycles of P-wave energy. This minimized contamination by secondary arrivals. All pairs of windowed traces for a given earthquake were cross-correlated and relative arrival-times Δt_{ij} between pairs of stations i,j were obtained [*VanDecar and Crosson*, 1990]. Relative arrival-

Table 1. List of Seismograph Stations Used in the Study[a]

Site Code	Latitude	Longitude	Elevation (m)	Network	Sensor
ACCN	43.3843	−73.6678	340	LCSN	CMG-3T (BB)
ALGO	45.9544	−78.0509	235	POLARIS	CMG-3ESP (BB)
BANO	45.0198	−77.9280	360	POLARIS	CMG-3ESP (BB)
BELQ	47.3980	−78.6874	355	POLARIS-UQAM	CMG-3ESP (BB)
BUKO	45.4423	−79.3989	317	POLARIS	CMG-3ESP (BB)
CHGQ	49.9105	−74.3748	406	POLARIS-UQAM	CMG-3ESP (BB)
CRLO	46.0375	−77.3801	168	CNSN	S-13 (SP)
DAQ	47.9644	−71.2425	939	CNSN	S-13 (SP)
DMCQ	48.9646	−72.0680	197	POLARIS-UQAM	Trillium120 (BB)
DPQ	46.6805	−72.7773	167	CNSN	S-13 (SP)
EEO	46.6411	−79.0733	398	CNSN	S-13 (SP)
FFD	43.4701	−71.6533	131	NESN	CMG-40T (BB)
FRNY	44.8350	−73.5883	223	LCSN	STS-2 (BB)
GAC	45.7033	−75.4783	62	CNSN	STS-1 (BB)
GRQ	46.6067	−75.8600	290	CNSN	S-13 (SP)
HSMO	47.3708	−79.6657	306	POLARIS	CMG-3ESP (BB)
KAPO	49.4504	−82.5079	210	CNSN	CMG-3ESP (BB)
KILO	48.4970	−79.7233	322	POLARIS/CNSN	CMG-3ESP (BB)
LATQ	47.3836	−72.7819	163	POLARIS-UQAM	CMG-3ESP (BB)
LG4Q	53.6269	−74.0972	168	CNSN	S-13 (SP)
LSQQ	49.0580	−76.9796	308	POLARIS-UQAM	Trillium120 (BB)
MALO	50.0244	−79.7635	271	POLARIS/CNSN	CMG-3ESP (BB)
MATQ	49.7589	−77.6376	280	POLARIS-UQAM	CMG-3ESP (BB)
MDV	43.9992	−73.1812	134	LCSN	HS-10 (SP)
MOQ	45.3120	−72.2541	841	CNSN	S-13 (SP)
MRHQ	45.8870	−74.2127	422	POLARIS	CMG-3ESP (BB)
MSNO	51.2913	−80.6113	4	POLARIS	CMG-3ESP (BB)
NEMQ	51.6837	−76.2576	197	POLARIS-UQAM	CMG-3ESP (BB)
NMSQ	51.7133	−76.0237	275	POLARIS-UQAM	CMG-3ESP (BB)
OTRO	50.1818	−81.6286	109	POLARIS	CMG-3ESP (BB)
PECO	43.9340	−76.9939	92	POLARIS	CMG-3ESP (BB)
PEMO	45.6773	−77.2466	180	POLARIS	CMG-3ESP (BB)
PKME	45.2644	−69.8917	109	US	STS-2 (BB)
PLVO	45.0396	−77.0754	279	POLARIS	CMG-3ESP (BB)
PQI	46.6710	−68.0168	180	NESN	CMG-40T (BB)
QCQ	46.7789	−71.2758	91	CNSN	CMG-3ESP (BB)
RSPO	46.0734	−79.7602	264	POLARIS	CMG-3ESP (BB)
SUNO	46.6438	−81.3442	369	POLARIS/CNSN	CMG-3ESP (BB)
TIMO	48.4659	−81.3032	392	POLARIS	CMG-3ESP (BB)
TRQ	46.2222	−74.5556	853	CNSN	S-13 (SP)
VLDQ	48.1124	−77.4536	93	CNSN	CMG-3R (BB)
WBO	45.0003	−75.2750	85	CNSN	S-13 (SP)
WCNY	43.9810	−75.6549	245	LCSN	CMG-3ESP (BB)
WEMQ	53.0535	−77.9737	172	POLARIS	CMG-3ESP (BB)
WLVO	43.9236	−78.3970	70	POLARIS	CMG-3ESP (BB)
WVL	44.5648	−69.6575	85	NESN	CMG-40T (BB)
YOSQ	52.8666	−72.1998	649	POLARIS	CMG-3ESP (BB)

[a]CNSN: Canadian National Seismograph Network, POLARIS: Portable Observatories for Lithospheric Analysis and Research Investigating Seismicity, UQAM: Université du Québec à Montréal, LCSN: Lamont Cooperative SeismographicNetwork, NESN: New England Seismic Network, US: United States National Seismic Network. Negative longitudes represent degrees West. BB: broadband sensor, SP: short-period sensor.

times for each station were then retrieved by a least-squares minimization of the residual res_{ij} for all station pairs where:

$$res_{ij} = \Delta t_{ij} - \left(t_i - t_j\right), \tag{1}$$

where t_i and t_j are the arrival-times associated with the ith and jth traces respectively.

[22] Relative arrival-time residuals t_{RES} for each station are then given by:

$$t_{RES_i} = t_i - (t_{e_i} - \overline{t_e}), \tag{2}$$

where t_i is the relative arrival-time for each station i; t_{e_i} is the expected travel-time based on the IASP91 travel-time tables [*Kennett and Engdahl*, 1991] for the ith station and $\overline{t_e}$ is the mean of the IASP91 theoretical travel-times associated with that particular earthquake.

[23] The MCCC method also provides a means of quantifying the error associated with each arrival-time. The standard deviation σ_i of the distribution of the residuals (res_{ij}) associated with the ith trace is determined by:

$$\sigma_i = \sqrt{\frac{1}{(n-2)}\sum_{j \neq i} res_{ij}^2}, \tag{3}$$

[24] In this study relative arrival-times determined in this way have mean standard deviation 0.02 s. In line with the studies of *Bastow et al.* [2005] and *Tilmann et al.* [2001] we regard the MCCC-derived estimates of timing uncertainty as optimistic. Our final data set of relative arrival-time residuals

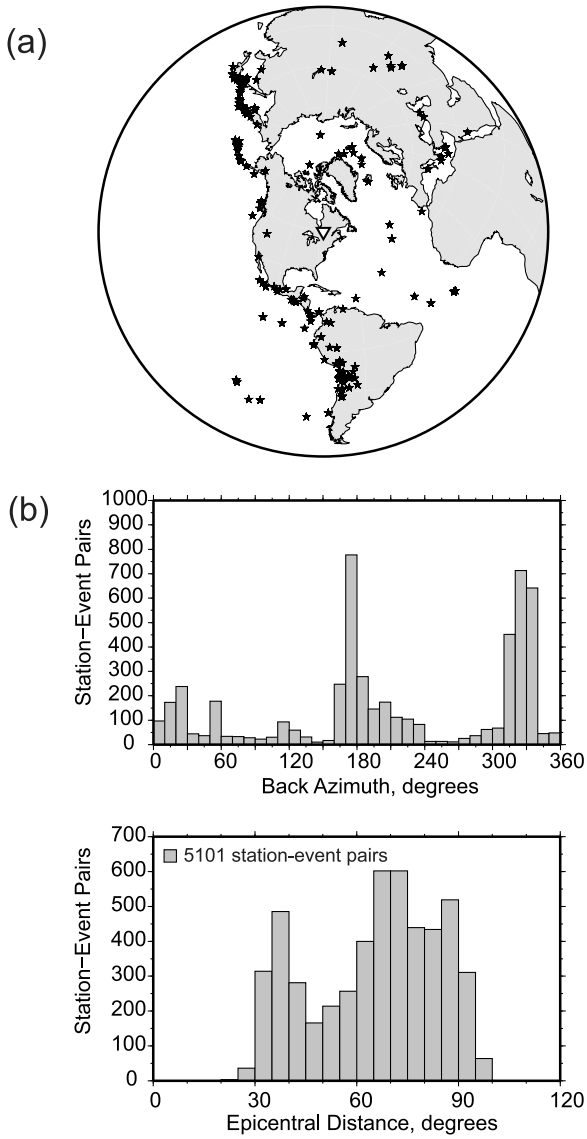

Figure 2. (a) Distribution of earthquakes used for travel-time analysis in this study. (b) Histograms showing the distributions of (top) back-azimuth and (bottom) epicentral distance for the >5100 event-station pairs analyzed.

comprises ~5100 earthquake–station pairs, whose distribution as a function of back azimuth and epicentral distance is shown in Figure 2.

2.3. Analysis of Travel-Time Residuals

[25] When interpreting body-wave tomographic images it is vital to appreciate whether absolute or relative arrival-times have been used to construct them. While absolute delay times enable the determination of seismic heterogeneities compared to the global mean, relative arrival-time techniques such as that employed here carry no such information. The computation of relative arrival-time residuals (equation (2)) completely removes the background mean delay time for the region sampled by the network. Compilations of absolute travel-time data for continental seismograph stations worldwide [e.g., *Poupinet*, 1979] show that permanent stations within the Canadian Shield are characterized by some of the earliest teleseismic P-wave arrival-times on Earth. It must therefore be kept in mind that tomographic images generated from inversion of our relative arrival-time residuals will be superimposed on an absolute 'pedestal' that is markedly fast relative to the global average.

[26] Figure 3 shows a map of mean relative arrival-time residuals for our network. Stations in the Archean Superior craton exhibit consistently earlier (negative relative arrival-time residuals) arrivals than those within the younger Grenville and Appalachian terranes to the southeast. The latest arrivals (positive relative arrival-time residuals) are found at those stations closest to the continent-ocean boundary in the northeast US. Plots of the variations of relative arrival-time residuals at selected individual stations as a function of back azimuth and epicentral distance are shown in auxiliary material.[1]

2.4. Model Parameterization and Tomographic Inversion Procedure

[27] We use the regularized, least-squares tomographic inversion procedure of *VanDecar et al.* [1995] to invert our data set of P-wave relative arrival-time residuals for velocity perturbations beneath eastern Canada. P-wave slowness is parameterized using splines under tension over a dense grid of knots [*Cline*, 1981]. The equilateral grid consists of 27 knots in depth between 0 and 1300 km, 77 knots in latitude between 35° and 62°N and 85 knots in longitude between 54° and 96°W, for a total of 176,715 knots

[1]Auxiliary materials are available in the HTML. doi:10.1029/2012JB009639.

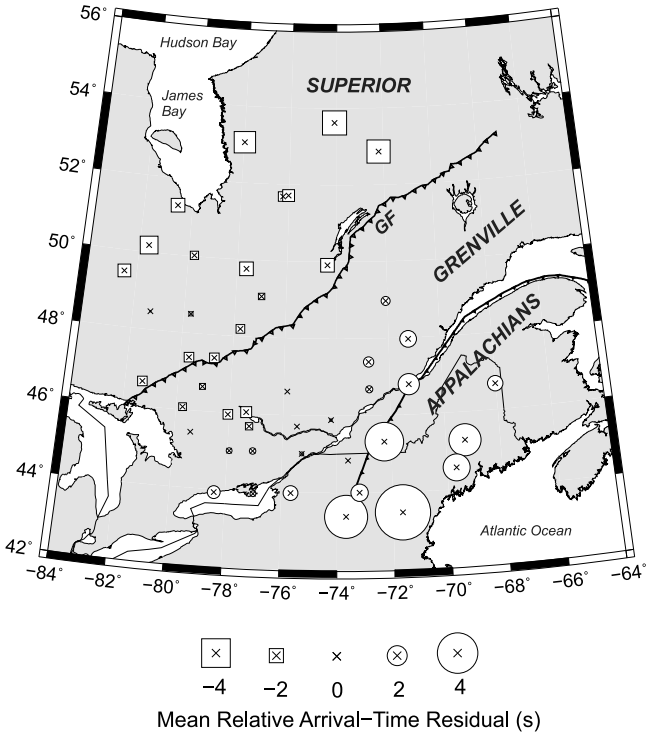

Figure 3. Mean relative arrival-time residuals for the seismograph network. Negative arrivals (squares) are early with respect to the regional average and positive arrivals (circles) are late.

parametrizing slowness. Knot spacing is ~30 km in the innermost resolvable parts of the model, increasing to ~50 km between 600 and 800 km depth, and ≥100 km from 800 to 1300 km depth. Tests have shown that the tomographic images we recover are independent of knot position.

[28] In the inversion procedure, we solve simultaneously for slowness perturbations, source static terms and station static terms. Source terms are free parameters in the inversion procedure that account for small variations in back azimuth and incidence angle caused by distant heterogeneities and hypocenter mislocations. The station terms account for travel-time anomalies associated with shallow structure (crust and uppermost mantle) directly beneath the station where a lack of crossing rays prevents resolution of crustal wave speeds.

[29] We regularize our under-determined (more unknowns than observations) inverse problem through the minimization of a 7-point finite element approximation to the Laplacian operator in order to penalize the roughness (second derivative) of the final slowness model. We thus choose to select a smooth model that contains the least amount of structure required to fit the data [e.g., *Constable et al.*, 1987; *VanDecar et al.*, 1995]. In addition, the outside knots in the model (with the exception of the top layer) are heavily damped to zero anomaly so that the 3D model merges smoothly into the surrounding radial Earth.

[30] By investigating the tradeoff between the RMS residual reduction (the percentage difference between the initial and final RMS misfit to the travel-time equations) and RMS model roughness (auxiliary material) we select a preferred model that fits the data well but does not account for more relative arrival-time residual reduction than can be justified by our MCCC-derived estimation of data noise levels (~0.02 s). Our P-wave model accounts for 93% (from 0.42 s to 0.03 s) of the RMS relative arrival-time residuals. We are thus treating our estimates of RMS timing uncertainty as optimistic bounds when fitting the data. Subtracting static terms from the travel-time data set reduces the RMS relative arrival-time residuals from 0.42 to 0.36 s; these corrected residuals more accurately reflect the proportion of the delay time anomalies that will be mapped into the mantle, where we make our structural interpretations.

3. Resolution

[31] We test the resolving power of our data set by analyzing its ability to retrieve synthetic anomalies. Two models are tested: a standard checkerboard and a structural model based on inferences from the geological record and previous geophysical investigations of the study region.

[32] In the checkerboard test, we place positive and negative anomaly ($\delta Vp = \pm 5\%$; 75 km diameter) spheres described by Gaussian functions across their diameter in layers at 150, 350, 550, 750, and 950 km depth. We invert for the synthetic velocity structure using the same model parameterization and inversion regularization parameters as used in the inversion of the observed data. A Gaussian residual time error component with a standard deviation of 0.02 s (the MCCC-derived error estimate for the observed data) is added to the synthetic travel times prior to inversion. Figure 4 shows the synthetic model and the recovered velocity structure from the checkerboard test. In the depth slices, the spheres are distinct from one another throughout the upper mantle and into the mid-mantle. Lateral resolution and the recovery of the amplitudes of the velocity anomalies is best at 350 km where we expect a seismograph network of our dimensions to have the highest density of crossing rays [e.g., *Ritsema et al.*, 1998]. Some vertical smearing of the anomalies does occur, as is common in this type of body-wave tomographic inversion.

[33] Our second synthetic test consists of a slow-wave speed anomaly (defined by a Gaussian function across its width) along the proposed Great Meteor hot spot track, extending at peak anomaly ($\delta Vp = -5\%$) to 150 km depth and falling to zero anomaly at ~200 km depth (Figure 5). In addition, a similarly-defined high-wave speed anomaly is placed in the northern part of the study area, in the region where seismic reflection images suggest the presence of an Archean subducted slab [*Calvert et al.*, 1995]. If the slab extends to depth and remains embedded in the Superior lithospheric root, we might see a high-velocity anomaly in our P-wave model, such as that inferred by *Sol et al.* [2002] in the western Superior. The low-velocity Great Meteor hot spot track anomaly is retrieved with limited vertical smearing, and with little lateral offset from its original location (Figure 5). Notably, there is no deterioration in resolution of the low-velocity anomaly across the Superior–Grenville boundary. Recovered amplitudes drop off further north within the Superior craton, and to the south in the Appalachians towards the continent-ocean boundary. The fast-wave speed anomaly further north is not retrieved with the same degree of success, smearing to almost 500 km depth, but its lateral resolution is good (Figure 5).

4. The 3D P-Wave Velocity Model

[34] Figure 6 shows a low-wave speed anomaly of $\delta Vp \approx -1\%$, most prominent at depths of 100–300 km, beneath the Appalachian region of our network. Low velocities at these depths follow a WNW–ESE trend along the proposed Great Meteor hot spot track (Figure 1) into the Grenville province, but terminate abruptly at the Grenville–Superior boundary. Our synthetic tests (Figures 4 and 5) show that this is a robust model feature. Cross-sections through the low-wave speed anomaly (Figure 7: C-C') within the Grenville province show that the feature is narrow (no more than ~120 km wide) with sharp sides, and constrained to the upper ~250 km. To the southeast, the low-velocity body broadens significantly. The lowest velocities correlate with the White Mountains of the northeast US and extend towards the offshore region of the New England seamounts (Figure 1). These observations are also robust on the basis of our resolution tests (Figures 4 and 5).

[35] Except for the region affected by the Great Meteor hot spot, the Grenville and Superior provinces are characterized by seismic velocities close to or higher than the regional average ($\delta Vp \geq 0$) at lithospheric depths. A peak anomaly ~300 km aperture body is observed in the northernmost part of the study area beneath the Opatica domain (Figure 1). Although checkerboard tests (Figure 4) suggest that this region is not well-resolved in the model, structural tests (Figure 5) do suggest that a fast anomaly can be identified. Section C–C′ suggests that high velocities in the depth range 0–200 km in this region would be expected to smear to

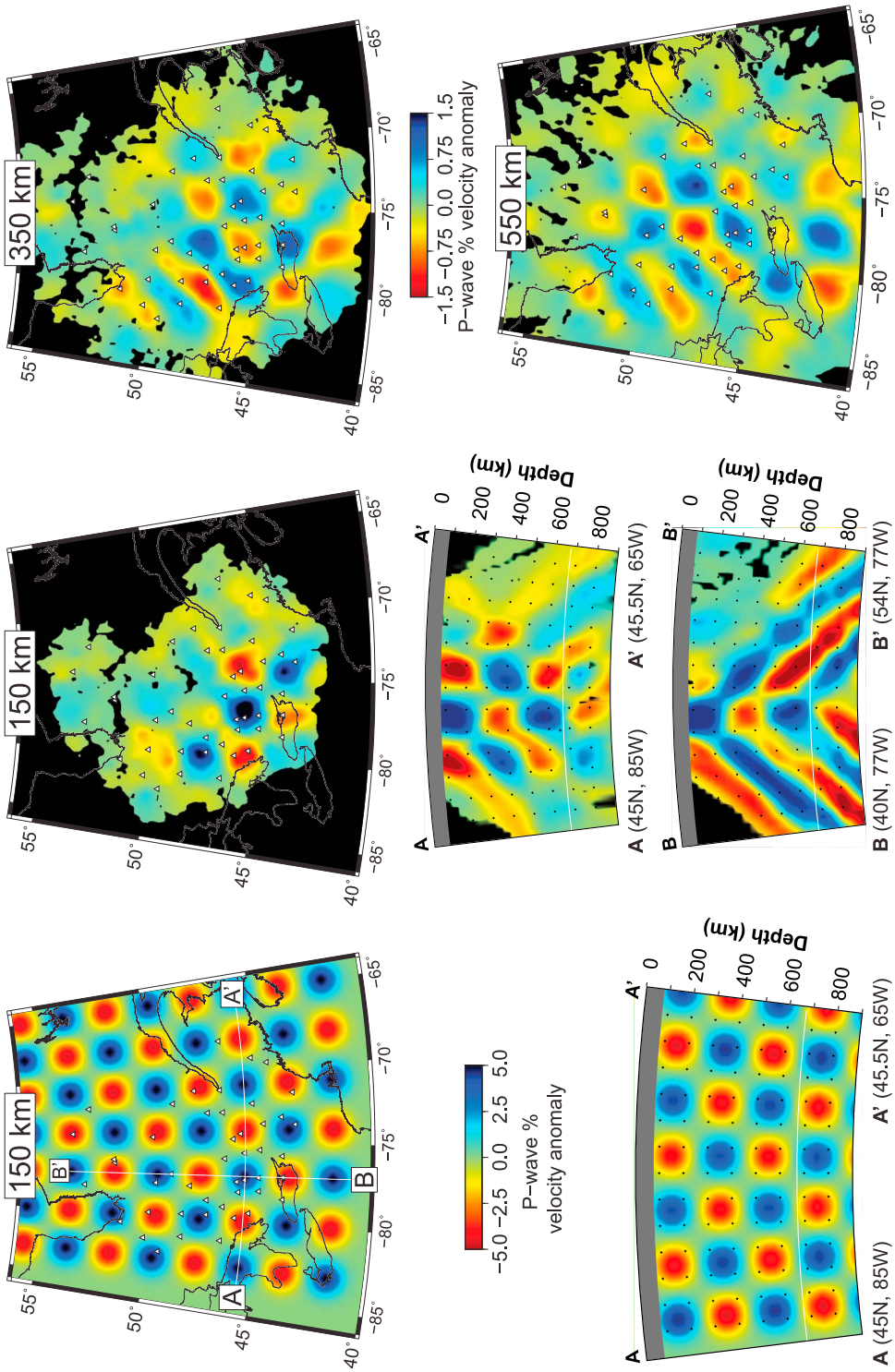

Figure 4. Cross-sections and depth slices through the synthetic checkerboard model used to assess resolution. The input checkerboard consists of alternating high- and low-velocity anomalies (defined by Gaussian functions across their diameter) of 75 km diameter and ±5% peak amplitude. The output models show how these anomalies are recovered for the raypath distribution of the travel-time data set. A peak amplitude of ±1.5% is recovered. Areas of low ray density are black, and the grey band at the top of the cross-sections shows the depth range for which no resolution is expected due to a lack of crossing raypaths.

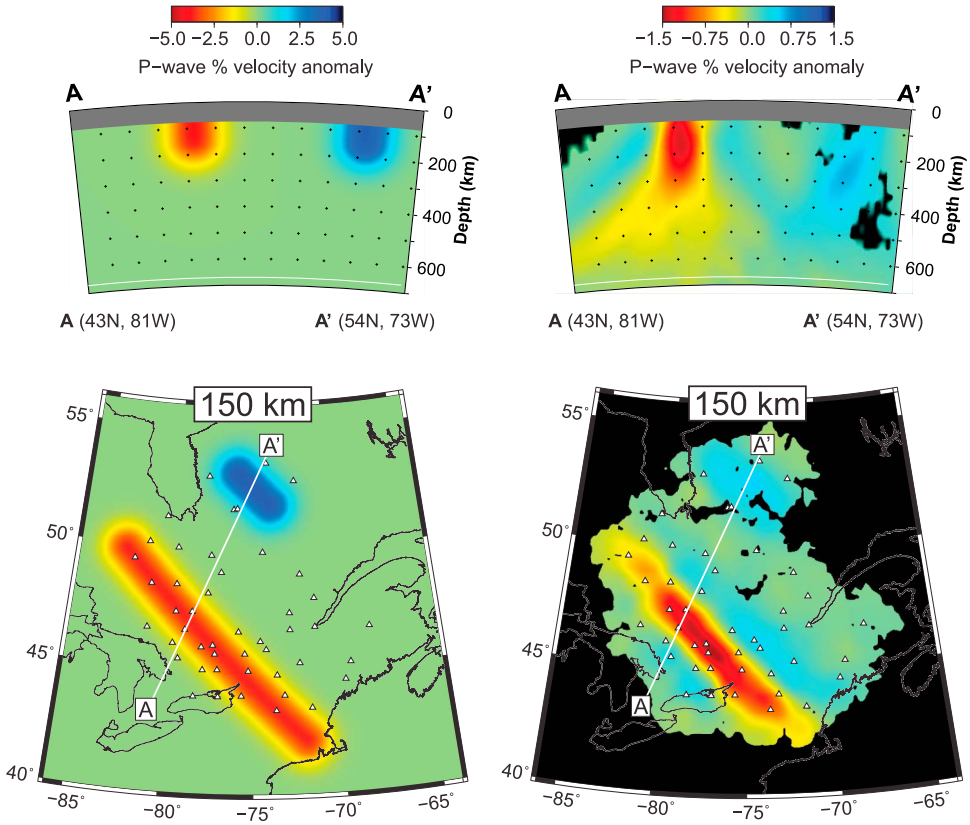

Figure 5. Cross-sections and depth slices through the structural resolution test. The input model consists of a low-velocity corridor and a high-velocity body (defined by Gaussian functions across their width), both residing in the top 200 km; peak amplitudes down to 150 km depth. The output model shows the recovery of the two anomalies, with a peak amplitude of ±1.5%. Plotting conventions as for Figure 4.

~450 km depth. In addition, tests of model smoothing (auxiliary material Figure S2) show that, even for the smoothest models, seismic velocities in this region are faster than elsewhere in the model.

[36] At sublithospheric depths, relatively low velocities are continuous throughout the upper mantle and through the transition zone beneath the southeasternmost part of the study area (Figure 6). In contrast, a high-wave speed NW–SE trending body north of ~46°N extends downwards from ~600 km depth and into the mid-mantle (Figures 6 and 7). This region of the model is not well resolved (Figures 4 and 5), so the morphology of the high-velocity anomaly feature is not considered to be well constrained. However, tests have shown that high wave speeds at this depth range in the model are independent of the depth of parameterization and of the chosen regularization parameters, and we therefore consider this anomaly to be a robust feature.

5. Discussion

5.1. Causes of Mantle Seismic Heterogeneity

[37] Prior to interpreting our tomographic images (Figures 6 and 7), it is vital to appreciate the significance of the δVp = 0% contours on our plots. As described in Section 2.3, our tomographic inversion of relative traveltimes results in models that illuminate wave speed variations with respect to the regional mean, not the global average [see, e.g., *Bastow*, 2012]. The mean seismic velocity anomaly in the upper 410 km of the global tomographic model of *Ritsema et al.* [2011] for the 47 seismograph stations used in this study is $\delta V_S \approx +1.6\%$, implying that the mean velocity structure in our study area is markedly fast compared to the global average. Therefore, even red (relatively low wave speed) regions of Figures 6 and 7 are likely fast compared to the global mean, except near the coast, where the Appalachian mantle may be genuinely slightly slow compared to the global average [e.g., *van der Lee and Frederiksen*, 2005; *Bedle and van der Lee*, 2009].

[38] At upper mantle depths, temperature is usually assumed to be the principal control on seismic heterogeneity, with compositional effects assigned only a subordinate role in interpreting tomographic images [e.g., *Karato*, 1993; *Goes et al.*, 2000; *Cammarano et al.*, 2003; *Faul and Jackson*, 2005]. Compositional effects can also be important, however [e.g., *Deschamps et al.*, 2002; *Artemieva et al.*, 2004]. Depletion of the sub-continental lithospheric mantle of lower melting-point components can cancel thermal effects on density [e.g., *Jordan*, 1988] and, by inference, seismic velocity.

[39] The youngest magmatism known to have affected our study area is that associated with the ~160–110 Ma passage of the Great Meteor hot spot, which affected the Superior, Grenville and Appalachian terranes (Figure 1). Thermal models examining the effects of upward cooling and lateral diffusion suggest that, for an initial hot spot-related temperature anomaly of 100–150°C in the mantle below the

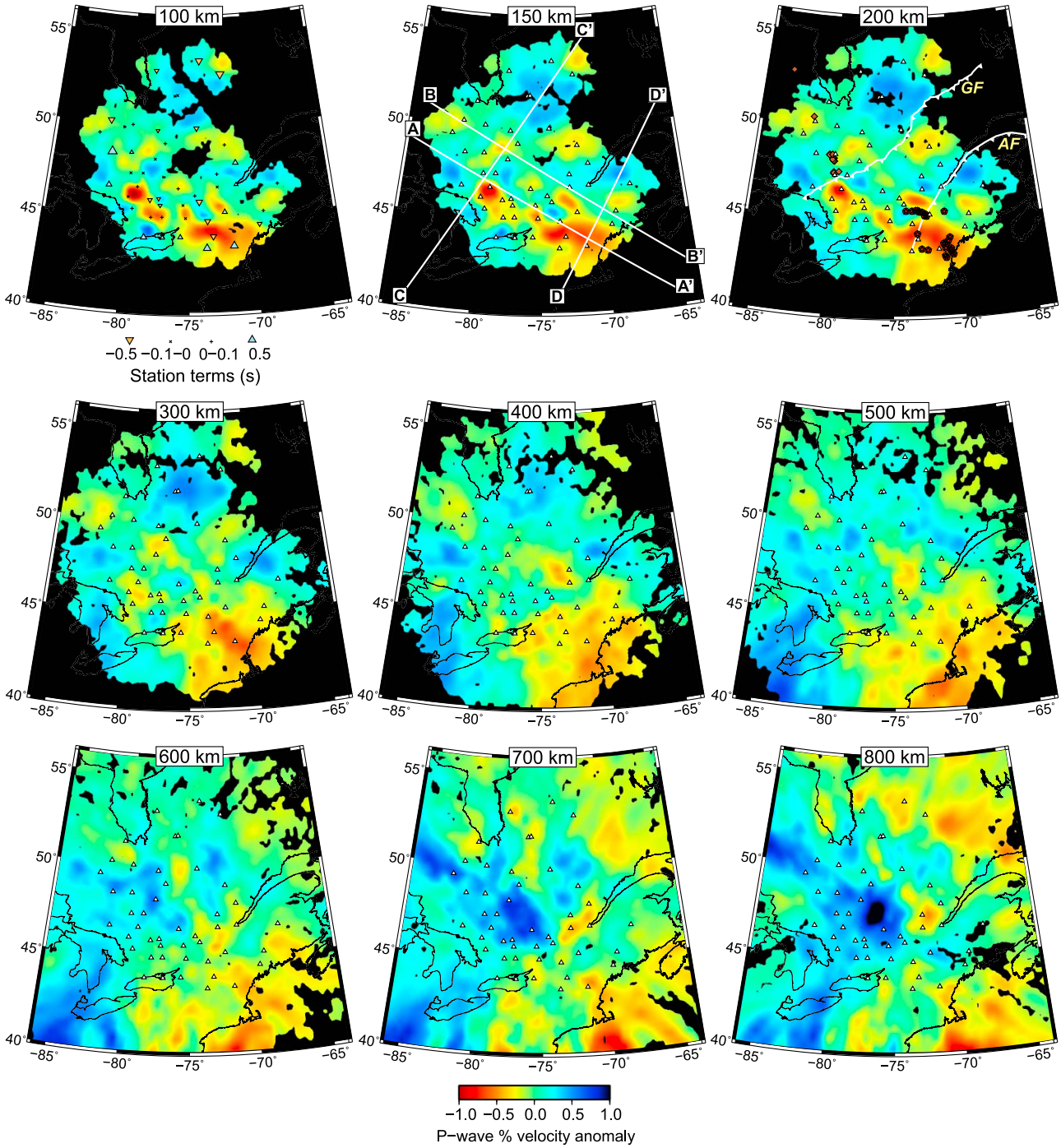

Figure 6. Depth slices through the final model throughout the upper mantle, transition zone and mid-mantle. Station locations are shown as small white triangles. Station static correction terms are shown in the 100 km depth slice, and locations of cross-sections (Figure 7) are shown as white lines on the 150 km depth slice. On the 200 km depth slice, white lines with tick marks show the positions of the Grenville and Appalachian Fronts (GF and AF respectively); brown diamonds show Cretaceous kimberlite eruptions and red circles/stars show Cretaceous intrusive magmatism. Plotting conventions as for Figure 4.

continental lithosphere, the residual temperature anomaly after ~100 My would be no more than ~50°C and the temperature perturbation would have spread laterally in the mantle [e.g., *Eaton and Frederiksen*, 2007]. Such a small thermal signature would produce a P-wave speed reduction of <0.3% in the lithospheric mantle, assuming minimal anelastic effects [e.g., *Nataf and Ricard*, 1996; *Goes et al.*, 2000]. Consistent with this, heat flow studies from the region indicate low heat flow across the Precambrian Superior and Grenville provinces (generally ≤50 m Wm^{-2} [e.g., *Lévy et al.*, 2010]). Short wavelength, low amplitude variations in heat flow are attributed in these studies to variations

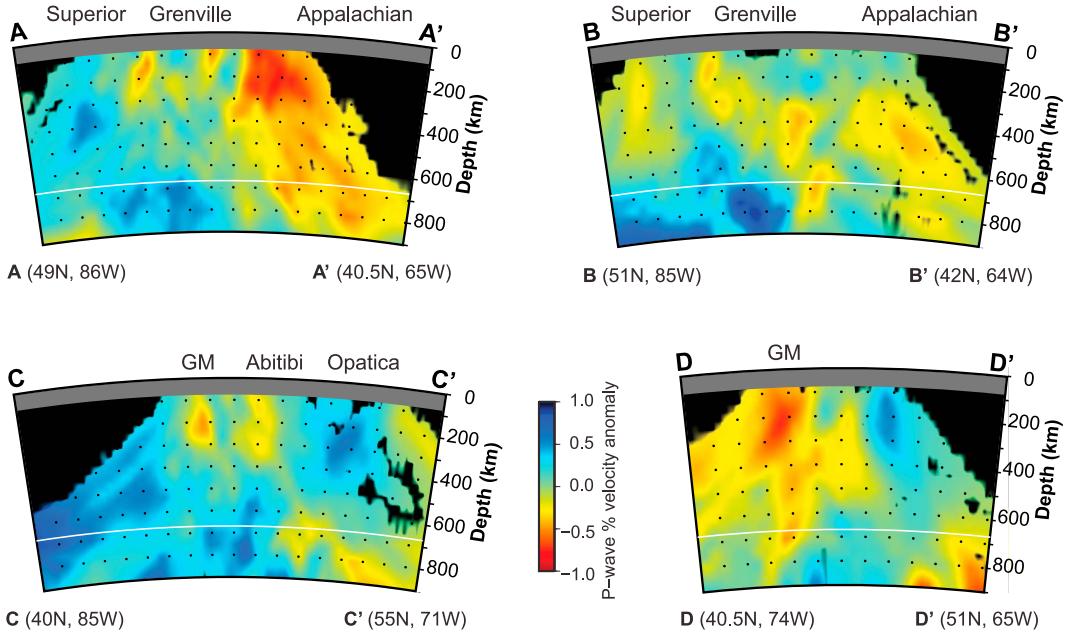

Figure 7. Cross sections through the final model; see Figure 6 for locations. A-A′: along the low-velocity corridor, B-B′: along the maximum of the deep high-velocity anomaly, C-C′: across the low-velocity corridor and shallow high-velocity anomaly, D-D′: across the broader low-velocity zone beneath the Appalachian region. GM: Great Meteor hot spot (interpretation of low-velocity corridor).

in crustal radiogenic heat production, with no requirement for short-wavelength variability in mantle heat flux. Thus, within the lithosphere beneath our study area the absence of young tectonic activity should mean that the effect of temperature on seismic wave speed is largely negligible.

[40] The geometry of low-velocity anomalies in tomographic images also provides clues as to the cause of the seismic heterogeneity. While thermal anomalies would be expected to diffuse laterally over time, compositional anomalies can retain sharp boundaries over millions of years [e.g., *Garnero et al.*, 2007]. Below the lithosphere, it is expected that temperature variations will dominate the seismic heterogeneity revealed in our tomographic models.

[41] In the following sections we use our tomographic images to shed new light on the processes that formed and shaped the lithosphere of eastern North America in Precambrian times, and how magmatism (principally due to the Great Meteor hot spot) has subsequently modified it.

5.2. Comparison Between Archean, Proterozoic and Paleozoic Upper Mantle

[42] Throughout the Precambrian it is expected that the processes responsible for the formation of continental lithosphere evolved as Earth cooled and modern-style plate tectonics began. In the broadest sense, this is well established seismologically in that the mantle beneath the shields is characterized by elevated seismic wave speeds compared to younger Phanerozoic mantle. The high wave speeds beneath the cratons are usually explained in the context of a depleted composition [e.g., *Jordan*, 1988].

[43] In southern Africa, Archean domains are usually characterized by faster seismic wave speeds than surrounding younger Proterozoic mobile belts [e.g., *Li and Burke*, 2006; *Chevrot and Zhao*, 2007], with the implication that mantle composition and/or plate formation processes evolved between Archean and Proterozoic times. In contrast, in Australia, there is no clear distinction between Archean and Proterozoic mantle lithospheric wave speed structure [e.g., *Simons et al.*, 1999; *Fishwick et al.*, 2005]. The same is true for Fennoscandia [e.g., *Bruneton et al.*, 2004], whereas *Lebedev et al.* [2009] found systematically slower wave speeds beneath the Proterozoic fold belts of central Asia compared to the cratonic Russian platform.

[44] The tectonic history of our study area spans ~3 Ga of the geological record, from Archean formation of the Superior craton to the Paleozoic accretion of the Appalachian terranes to Laurentia. Our tomographic images thus provide an excellent opportunity to test whether there is a systematic age-dependence on seismic wave speed anomalies.

[45] Faster wave speeds are generally observed beneath the Precambrian (Superior and Grenville) than the Paleozoic (Appalachian) terranes (Figure 6), as is commonly observed between Phanerozoic and Precambrian regions worldwide. At first inspection, our observations of variation of mean relative arrival-time residuals in the Superior and Grenville provinces also suggest that seismic wave speed characteristics may be different between Archean and Proterozoic lithosphere. However, the tomographic images (Figure 6) are less convincing, with no obvious systematic variation in seismic wave speed across the boundary between the two provinces. Heat flow data, which also show no systematic age-dependence, corroborate this observation [e.g., *Mareschal et al.*, 2000]. Tectonic stabilization of cratons may have thus occurred in a similar fashion between the Archean and Proterozoic. Alternatively, we cannot preclude the possibility that much of the lithospheric mantle beneath the Grenville province is, in fact, Archean in age. Indeed, *White et al.* [2000] proposed on the strength of evidence from

Lithoprobe wide-angle seismic data that a substantial volume of Superior mantle likely underlies the Grenville province.

[46] In general, we note a similar magnitude of seismic wave speed variation within lithospheric subdivisions of the Canadian Shield as across their boundaries (Figures 6 and 7). In particular, we note the broad high-wave speed anomaly situated beneath the Opatica/Opinaca region (Figure 1). Our resolution tests (Figure 5) and smoothing tests (auxiliary material Figure S2) suggest that this is likely a robust feature, but that its extension to ~400 km depth arises from vertical smearing. Instead, the anomaly is more likely embedded in the Superior lithosphere. There is considerable speculation about the preservation of Archean subduction processes based on seismic reflection studies of this part of the Superior craton [e.g., *Calvert et al.*, 1995; *Clowes*, 2010] and previous interpretations of high-velocity features within the Canadian Shield as slab remnants [e.g., *Sol et al.*, 2002; *Aktas and Eaton*, 2006; *Frederiksen et al.*, 2007]. It is therefore tempting to interpret this anomaly as a slab remnant; however a more detailed regional analysis than that possible here is needed to improve constraint on the geometry and extent of the anomaly.

5.3. The Impact of Hot Spot Tectonism on Archean-to-Paleozoic Age Lithosphere

[47] The Great Meteor hot spot track extends from Nunavut, northern Canada, southeast through our study area (Figure 1), and offshore from the eastern US, where it is preserved as a chain of seamounts. Our observations of low-velocity anomalies in the lithospheric mantle beneath the hot spot track in the Grenville province and Appalachian terranes suggest strongly that Great Meteor magmatism has imparted a compositional signature on the North American lithosphere.

[48] In geodynamic models, the thickness and geometry of continental lithosphere has been shown to have a significant effect on the flow of plume material and the nature of its interaction with the lithosphere. The thick, stable cratonic keels generally deflect the flow of plume material towards regions of thinner lithosphere [e.g., *Sleep*, 1997]. If the plume center lies directly beneath a stable cratonic keel, some of the material may be able to pond beneath the cratonic lithosphere, but magmatism is restricted to small-volume melts derived from depths of over 150 km [e.g., *Ebinger and Sleep*, 1998; *Sleep et al.*, 2002]. Thinning of the cratonic lithosphere as a result of direct interaction with the plume center is modest, and the craton remains stable and resistant to pervasive modification [e.g., *Sleep*, 2003]. More significant ponding of plume material occurs in zones where the lithosphere is thinner, due to the deflection of buoyant asthenosphere away from the cratonic keels. Where steep gradients in lithospheric thickness are present, the focusing of plume flow may enhance melting and magmatism [e.g., *Ebinger and Sleep*, 1998; *Sleep et al.*, 2002]. Variations in lithospheric strength may also play a role in the nature of plume-lithosphere interaction. While rift-related structures in cratonic regions may not necessarily cause significant lithospheric thinning [e.g., *Petit and Ebinger*, 2000], they are likely to weaken the lithosphere, act as stress guides, and focus strain. Magmatic material from a plume impinging on the lithosphere may therefore be more able to penetrate weak zones arising from earlier rifting episodes in continental lithosphere, and would be focused preferentially on these zones [e.g., *Burov et al.*, 2007].

[49] Much of our study region is underlain by a thick cratonic keel [e.g., *Nettles and Dziewonski*, 2008]. Regional body-wave tomography studies are not able to constrain the geometry of the keel nor identify the lithosphere-asthenosphere boundary, but the high-wave speed signature of the North American craton is clearly visible in seismic surface-wave studies. The keel appears to extend beneath both the Archean and Grenville provinces, to a depth of ~200–250 km, with the exception of the 'divot' beneath the lower Great Lakes region [e.g., *Bedle and van der Lee*, 2009; *Nettles and Dziewonski*, 2008]. In contrast, the inferred lithospheric thickness beneath the younger Appalachian terranes is typically between 100 and 150 km in most seismic models. Effective elastic thickness, a proxy for lithospheric strength [e.g., *Pérez-Gussinyé et al.*, 2009], is high (>100 km) beneath the Canadian Shield and relatively low (<80 km) beneath the Appalachians; however the resolution of the elastic thickness models is insufficient to identify local variations within the Shield [*Audet and Bürgmann*, 2011].

[50] Northwest of the Grenville–Superior boundary, the Archean portion of our study area shows no evidence for low wave speed anomalies along the proposed Great Meteor hot spot track. The only record of the hot spot magmatism in the Superior craton is the presence of kimberlite pipes [e.g., *Heaman and Kjarsgaard*, 2000]. Kimberlite melts are typically small in volume, developing deep within the mantle before rising rapidly towards the surface, causing little modification of the mantle lithosphere en route. The nature of the magmatism, together with the lack of any discernible seismic signature of lithospheric modification along the hot spot track in this region is consistent with the idea of the cratonic keels being intrinsically resistant to pervasive modification or erosion via interaction with plumes, due to their distinct composition, buoyancy and thickness [e.g., *Sleep et al.*, 2002].

[51] Within the upper mantle beneath the Grenville Province, a pronounced low-velocity anomaly is visible in our tomographic model. The anomaly has a restricted width of ≤120 km and sharp boundaries (a change of >0.8% anomaly over ~20 km; Figures 6 and 7). The sharpness of the anomaly boundaries is consistent with a dominantly compositional rather than thermal signature [e.g., *Garnero et al.*, 2007]. The Mesozoic magmatic record of the Grenville province is dominated by episodic alkaline magmatism, in particular the intrusive complexes of the Monteregian Hills of Québec [e.g., *Eby*, 1987]. Much of the Grenville lithosphere appears to have a cratonic signature on a large scale; however the region where we observe the low wave speed anomaly is the site of a late Precambrian failed rifting episode associated with the breakup of Rodinia and the opening of the Iapetus ocean. The degree to which the failed rifts thinned the lithosphere in the late Precambrian is uncertain, as is the extent to which post-rifting cooling of the mantle could have resulted in lithosphere of similar thickness to the surrounding cratonic lithosphere. Whether or not the hot spot magmatism in this region was the result of buoyant asthenosphere flowing along regions of thinned lithosphere

is difficult to prove unambiguously. Regardless of the effect of LAB topography on the asthenospheric flow at the time of the Great Meteor hot spot, ~400 My after the failed rifting episode, it is likely that late Precambrian rifting resulted in long-term weakening of this part of the cratonic keel [e.g., *Petit and Ebinger*, 2000]. A pre-existing weak zone of this type in the lithosphere may have acted as a stress guide to focus plume-related magmatism during the passage of the Great Meteor hot spot over 400 My later, allowing fertile melts to penetrate the depleted continental keel along a narrow zone.

[52] Low-velocity anomalies in the tomographic model are broadest and most pronounced within the Paleozoic Appalachian lithosphere, where hot spot-related magmatism is more silicic and voluminous than that of the Grenville province, with widespread plutonism in the White Mountains region [e.g., *Eby*, 1987]. The younger, thinner lithosphere was likely less resistant to hot spot-related modification than the stable cratonic keel, resulting in a pervasive seismic and geologic signature of the hot spot magmatism. In addition, the transition from thick cratonic to thin Phanerozoic lithosphere may have been sufficiently abrupt to focus plume flow and enhance mantle melting [e.g., *Sleep et al.*, 2002; *Burov et al.*, 2007].

[53] Comparison between the location of the low-velocity corridor beneath the Grenville Province, the position of surface magmatic features and plate-tectonic reconstructions of the likely track of the Great Meteor hot spot shows an east-west offset of up to 200–300 km. Though the resolution of the tomographic studies is significantly different, this result agrees broadly with the findings of *Eaton and Frederiksen* [2007], who proposed lateral deformation of the base of the lithospheric keel by asthenospheric flow.

5.4. Present-Day Subduction Processes

[54] Although not well resolved, the deepest portions of our velocity model (≥600 km) are dominated by a large high-wave speed anomaly which cannot easily be explained by smearing of upper mantle features (Figures 4 and 5). We therefore speculate that this high velocity anomaly may be the result of the subducting Farallon–Kula slab system beneath eastern North America. A high-velocity mid-mantle slab anomaly appears in several continent-to-global scale tomographic models [*Grand et al.*, 1997; *Li et al.*, 2008; *Forte et al.*, 2010; *Sigloch*, 2011]. The appearance of the high-wave speed anomaly as shallow as 600 km depth in our images is probably an effect of upward smearing in the tomographic model; instead, the feature is more likely confined below the transition zone. Supporting evidence can be found from studies of transition-zone thickness for the region, using receiver functions [e.g., *Li et al.*, 1998; *Thompson et al.*, 2011] or SS- and PP-precursors [e.g., *Lawrence and Shearer*, 2008; *Deuss*, 2009]. The transition zone in our region of interest does not appear significantly thickened with respect to the global average, nor is there evidence for a transition-zone thermal anomaly that would depress the 660 km discontinuity, suggesting that the Farallon slab would be a mid-mantle feature in this region.

[55] Another feature of global-scale mantle geodynamic models for eastern North America is the broad low-velocity anomaly we observe to the east of cratonic North America (Figures 6 and 7). *Forte et al.* [2010] predict that subduction of the Farallon–Kula slab beneath eastern North America should be driving a corner-flow influx of warmer, low-velocity anomaly mantle to fill the vacated space.

[56] Although the high-velocity mid-mantle anomaly does appear to be a robust feature in our model, we note that our interpretation is speculative, and requires more ambitious networks to confirm or rule out for this region. The imminent arrival of the EarthScope Transportable Array network in eastern North America should provide a sufficient array aperture to improve resolution in the deeper portions of the mid-mantle where the Farallon slab may reside.

6. Conclusions

[57] We have performed a teleseismic P-wave travel-time tomographic study of southeast Canada and the northeast US to illuminate mantle seismic heterogeneity beneath a region where the geological record spans ~3 Ga of Earth history.

[58] While there are no systematic differences in seismic wave speed across the boundary between Archean and Proterozoic provinces, the manner in which the lithosphere has been modified by Great Meteor hot spot magmatism shows a distinct change between the Superior, Grenville and Appalachian terranes. While modification of the Paleozoic Appalachian terrane is pervasive, the seismic signature of the hot spot in the Proterozoic Grenville province is much more localized. Beneath the oldest lithosphere in the study area, the Archean Superior craton, Great Meteor hot spot magmatism has had no discernible impact on lithospheric wave speed structure, consistent with the view that ancient Archean lithosphere has a higher preservation potential than younger Proterozoic and Phanerozoic lithosphere.

[59] **Acknowledgments.** Financial support for M.V. and F.D. was provided through NSERC Discovery Grants, FQRNT 'Établissement des nouveaux chercheurs', and UQAM 'PAFARC' funding programmes. I.B. is funded by the Leverhulme Trust. We are grateful to John VanDecar for making publicly available his tomographic inversion and MCCC codes. SAC [*Goldstein and Snoke*, 2005] and GMT [*Wessel and Smith*, 1998] software were also used in data analysis and preparation of the article. Seismic data were obtained from the IRIS DMC and from the Canadian National Data Centre (Natural Resources Canada). We thank the two reviewers, Stewart Fishwick and Cynthia Ebinger, for their helpful comments.

References

Aktas, K., and D. Eaton (2006), Upper-mantle velocity structure of the lower Great Lakes region, *Tectonophysics*, *420*, 267–281.

Allen, R., et al. (2002), Imaging the mantle beneath Iceland using integrated seismological techniques, *J. Geophys. Res.*, *107*(B12), 2325, doi:10.1029/2001JB000595.

Artemieva, I., M. Billien, J. Lévêque, and W. Mooney (2004), Shear-wave velocity, seismic attenuation, and thermal structure of the continental upper mantle, *Geophys. J. Int.*, *157*, 607–628, doi:10.1111/j.1365-246X.2004.02195.x.

Audet, P., and R. Bürgmann (2011), Dominant role of tectonic inheritance in supercontinent cycles, *Nat. Geosci.*, *4*, 184–187.

Bastow, I. (2012), Relative arrival-time upper-mantle tomography and the elusive background mean, *Geophys. J. Int.*, *190*, 1271–1278, doi:10.1111/j.1365-246X.2012.05559.x.

Bastow, I., G. Stuart, J.-M. Kendall, and C. Ebinger (2005), Upper-mantle seismic structure in a region of incipient continental breakup: Northern Ethiopian rift, *Geophys. J. Int.*, *162*, 479–493, doi:10.1111/j.1365-246X.2005.02666.x.

Bastow, I., A. Nyblade, G. Stuart, T. Rooney, and M. Benoit (2008), Upper mantle seismic structure beneath the Ethiopian hot spot: Rifting at the edge of the African low velocity anomaly, *Geochem. Geophys. Geosyst.*, *9*, Q12022, doi:10.1029/2008GC002107.

Bedle, H., and S. van der Lee (2009), *S* velocity variations beneath North America, *J. Geophys. Res.*, *114*, B07308, doi:10.1029/2008JB005949.

Bruneton, M., et al. (2004), Complex lithospheric structure under the central Baltic Shield from surface wave tomography, *J. Geophys. Res.*, *109*, B10303, doi:10.1029/2003JB002947.

Burov, E., L. Guillou-Frottier, E. d'Acremont, L. Le Pourhiet, and S. Cloetingh (2007), Plume head–lithosphere interactions near intra-continental plate boundaries, *Tectonophysics*, *434*, 15–38.

Calvert, A., E. Sawyer, W. Davis, and J. Ludden (1995), Archaean subduction inferred from seismic images of a mantle suture in the Superior Province, *Nature*, *375*, 670–674.

Cammarano, F., S. Goes, P. Vacher, and D. Giardini (2003), Inferring upper-mantle temperatures from seismic velocities, *Phys. Earth Planet. Inter.*, *138*, 197–222, doi:10.1016/S0031-9201(03)00156-0.

Chevrot, S., and L. Zhao (2007), Multiscale finite-frequency Rayleigh wave tomography of the Kaapvaal craton, *Geophys. J. Int.*, *169*, 201–215.

Cline, A. (1981), FITPAK – Software package for curve and surface fitting employing splines under tension, report, Dep. of Comput. Sci., Univ. of Tex. at Austin, Austin.

Clowes, R. (2010), Initiation, development, and benefits of Lithoprobe—Shaping the direction of Earth science in Canada and beyond, *Can. J. Earth Sci.*, *47*, 291–314.

Constable, S., R. Parker, and C. Constable (1987), Occam's inversion: A practical algorithm for generating smooth models from electromagnetic sounding data, *Geophysics*, *52*, 289–300.

Deschamps, F., J. Trampert, and R. Snieder (2002), Anomalies of temperature and iron in the uppermost mantle inferred from gravity data and tomographic models, *Phys. Earth Planet. Inter.*, *129*, 245–264.

Deuss, A. (2009), Global observations of mantle discontinuities using SS and PP precursors, *Surv. Geophys.*, *30*, 301–326.

Eaton, D., and A. Frederiksen (2007), Seismic evidence for convection-driven motion of the North American plate, *Nature*, *446*, 428–431.

Eaton, D., et al. (2005), Investigating Canada's lithosphere and earthquake hazards with portable arrays, *Eos Trans. AGU*, *86*, 169, doi:10.1029/2005EO170001.

Eaton, D., F. Darbyshire, R. Evans, H. Grütter, A. Jones, and X. Yuan (2009), The elusive lithosphere-asthenosphere boundary beneath cratons, *Lithos*, *109*, 1–22, doi:10.1016/j.lithos.2008.05.009.

Ebinger, C., and N. Sleep (1998), Cenozoic magmatism throughout east Africa resulting from impact of a single plume, *Nature*, *395*, 788–791.

Eby, G. (1987), The Monteregian Hills and White Mountain alkaline igneous provinces, eastern North America, *Geol. Soc. Spec. Publ.*, *30*, 433–447.

Ernst, R., and W. Bleeker (2010), Large igneous provinces (LIPs), giant dyke swarms, and mantle plumes: Significance for breakup events within Canada and adjacent regions from 2.5 Ga to the present, *Can. J. Earth Sci.*, *47*, 695–739.

Ernst, R., and K. Buchan (2001), The use of mafic dyke swarms in identifying and locating mantle plumes, *Spec. Pap. Geol. Soc. Am.*, *352*, 247–265.

Faul, U., and I. Jackson (2005), The seismological signature of temperature and grain size variations in the upper mantle, *Earth Planet. Sci. Lett.*, *234*, 119–134.

Fischer, K., H. Ford, D. Abt, and C. Rychert (2010), The lithosphere-asthenosphere boundary, *Annu. Rev. Earth Planet. Sci.*, *38*, 551–575, doi:10.1146/annurev-earth-040809-152438.

Fishwick, S., B. Kennett, and A. Reading (2005), Contrasts in lithospheric structure within the Australian craton—Insights from surface wave tomography, *Earth Planet. Sci. Lett.*, *231*, 163–176.

Forte, A., R. Moucha, N. Simmons, S. Grand, and J. Mitrovica (2010), Deep-mantle contibutions to the surface dynamics of the North American continent, *Tectonophysics*, *481*, 3–15, doi:10.1016/j.tecto.2009.06.010.

Frederiksen, A., S.-K. Miong, F. Darbyshire, D. Eaton, S. Rondenay, and S. Sol (2007), Lithospheric variations across the Superior Province, Ontario, Canada: Evidence from tomography and shear wave splitting, *J. Geophys. Res.*, *112*, B07318, doi:10.1029/2006JB004861.

Garnero, E., T. Lay, and A. McNamara (2007), Implications of lower-mantle structural heterogeneity for the existence and nature of whole-mantle plumes, *Spec. Pap. Geol. Soc. Am.*, *430*, 79–101.

Goes, S., R. Govers, and P. Vacher (2000), Shallow mantle temperatures under Europe from *P* and *S* wave tomography, *J. Geophys. Res.*, *105*, 11,153–11,169.

Goldstein, P., and A. Snoke (2005), SAC availability for the IRIS community, *IRIS DMC Newsl.*, *7*(1), Article 1. [Available at http://www.iris.edu/dms/newsletter/vol7/no1/sac-availability-for-the-iris-community/.]

Grand, S., R. van der Hilst, and S. Widiyantoro (1997), Global seismic tomography: A snapshot of convection in the Earth, *GSA Today*, *7*, 1–7.

Griffin, W., S. O'Reilly, and C. Ryan (1999), The composition and origin of sub-continental lithospheric mantle, *Spec. Publ. Geochem. Soc.*, *6*, 13–45.

Hatcher, R. D., Jr. (2005), Southern and central Appalachians, in *Encyclopedia of Geology*, edited by R. Selley, L. Cocks, and I. Plinner, pp. 72–81, Elsevier, Amsterdam.

Heaman, L., and B. Kjarsgaard (2000), Timing of eastern North American kimberlite magmatism: Continental extension of the Great Meteor hotspot track?, *Earth Planet. Sci. Lett.*, *178*, 253–268.

Hoffman, P. (1988), United plates of America, the birth of a craton: Early Proterozoic assembly and growth of Laurentia, *Annu. Rev. Earth Planet. Sci.*, *16*, 543–603.

Hopkins, M., T. Harrison, and C. Manning (2008), Low heat flow inferred from >4 Gyr zircons suggests Hadean plate boundary interactions, *Nature*, *456*, 493–496, doi:10.1038/nature07465.

Jordan, T. (1988), Structure and formation of the continental tectosphere, *J. Petrol.*, *1*, 11–37.

Karato, S. (1993), Importance of anelasticity in the interpretation of seismic tomography, *Geophys. Res. Lett.*, *20*(15), 1623–1626.

Kamo, S., T. Krogh, and P. Kumarapeli (1995), Age of the Grenville dyke swarm, Ontario-Quebec: Implication for the timing of Iapetan rifting, *Can. J. Earth Sci.*, *32*, 273–280.

Kennett, B., and E. Engdahl (1991), Travel times for global earthquake location and phase association, *Geophys. J. Int.*, *105*, 429–465.

King, S. (2005), Archean cratons and mantle dynamics, *Earth Planet. Sci. Lett.*, *234*, 1–14.

Lawrence, J., and P. Shearer (2008), Imaging mantle transition zone thickness with SdS-SS finite-frequency sensitivity kernels, *Geophys. J. Int.*, *174*, 143–158.

Lebedev, S., J. Boonen, and J. Trampert (2009), Seismic structure of Precambrian lithosphere: New constraints from broad-band surface-wave dispersion, *Lithos*, *109*, 96–111.

Lee, C., P. Luffi, and E. Chin (2011), Building and destroying continental mantle, *Annu. Rev. Earth Planet. Sci.*, *39*, 59–90.

Lekic, V., and B. Romanowicz (2011), Tectonic regionalization without a priori information: A cluster analysis of upper mantle tomography, *Earth Planet. Sci. Lett.*, *308*, 151–160.

Levin, V., A. Lerner-Lam, and W. Menke (1995), Anomalous mantle structure at the Proterozoic-Paleozoic boundary in the northeastern US., *Geophys. Res. Lett.*, *22*, 121–124.

Lévy, F., C. Jaupart, J.-C. Mareschal, G. Bienfait, and A. Limare (2010), Low heat flux and large variations of lithospheric thickness in the Canadian Shield, *J. Geophys. Res.*, *115*, B06404, doi:10.1029/2009JB006470.

Li, A., and K. Burke (2006), Upper mantle structure of southern Africa from Rayleigh wave tomography, *J. Geophys. Res.*, *111*, B10303, doi:10.1029/2006JB004321.

Li, A., K. Fischer, M. Wysession, and T. Clarke (1998), Mantle discontinuities and temperature under the North American continental keel, *Nature*, *395*, 160–163.

Li, A., D. Forsyth, and K. Fischer (2003), Shear velocity structure and azimuthal anisotropy beneath eastern North America from Rayleigh wave inversion, *J. Geophys. Res.*, *108*(B8), 2362, doi:10.1029/2002JB002259.

Li, C., R. van der Hilst, E. Engdahl, and S. Burdick (2008), A new global model for P wave speed variations in Earth's mantle, *Geochem. Geophys. Geosyst.*, *9*, Q05018, doi:10.1029/2007GC001806.

Ludden, J., and A. Hynes (2000), The Lithoprobe Abitibi-Grenville transect: Two billion years of crust formation and recycling in the Precambrian Shield of Canada, *Can. J. Earth Sci.*, *37*, 459–476.

Mareschal, J., C. Jaupart, C. Gariépy, L. Cheng, L. Guillou-Frottier, G. Bienfait, and R. Lapointe (2000), Heat flow and deep thermal structure near the southeastern edge of the Canadian Shield, *Can. J. Earth Sci.*, *37*, 399–414.

Nataf, H., and Y. Ricard (1996), 3SMAC: An a priori tomographic model of the upper mantle based on geophysical modelling, *Phys. Earth Planet. Inter.*, *95*, 101–122.

Nettles, M., and A. Dziewonski (2008), Radially anisotropic shear velocity structure of the upper mantle globally and beneath North America, *J. Geophys. Res.*, *113*, B02303, doi:10.1029/2006JB004819.

O'Reilly, S., and W. Griffin (2006), Imaging global chemical and thermal heterogeneity in the subcontinental lithospheric mantle with garnets and xenoliths: Geophysical implications, *Tectonophysics*, *416*, 289–309.

Percival, J. (2007), Geology and metallogeny of the Superior Province, Canada, in *Mineral Deposits of Canada: A Synthesis of Major Deposit-Types, District Metallogeny, the Evolution of Geological Provinces and Exploration Methods*, *Spec. Publ.*, vol. 5, edited by W. Goodfellow, pp. 903–928, Miner. Deposits Div., Geol. Assoc. of Canada, St. John's, Newfoundland, Canada.

Percival, J., M. Sanborn-Barrie, T. Skulski, G. Stott, H. Helmstaedt, and D. White (2006), Tectonic evolution of the western Superior province from NATMAP and Lithoprobe studies, *Can. J. Earth Sci.*, *43*, 1085–1117.

Pérez-Gussinyé, M., M. Metois, M. Fernández, J. Vergés, J. Fullea, and A. Lowry (2009), Effective elastic thickness of Africa and its relationship to other proxies for lithospheric structure and surface tectonics, *Earth Planet. Sci. Lett.*, *287*, 152–167.

Petit, C., and C. Ebinger (2000), Flexure and mechanical behavior of cratonic lithosphere: Gravity models of the East African and Baikal rifts, *J. Geophys. Res.*, *105*(B8), 19,151–19,162, doi:10.1029/2000JB900101.

Poupinet, G. (1979), On the relation between *P*-wave travel time residuals and the age of the continental plates, *Earth Planet. Sci. Lett.*, *43*, 149–161.

Ritsema, J., A. Nyblade, T. Owens, C. Langston, and J. VanDecar (1998), Upper mantle seismic velocity structure beneath Tanzania, East Africa: Implications for the stability of cratonic lithosphere, *J. Geophys. Res.*, *103*(B9), 21,201–21,213.

Ritsema, J., A. Deuss, H. van Heijst, and J. Woodhouse (2011), S40RTS: A degree-40 shear-velocity model for the mantle from new Rayleigh-wave dispersion, teleseismic traveltime and normal-mode splitting function measurements, *Geophys. J. Int.*, *184*, 1223–1236, doi:10.1111/1365-246X.2010.04884.x.

Rondenay, S., M. Bostock, T. Hearn, D. White, and R. Ellis (2000), Lithospheric assembly and modification of the SE Canadian Shield: Abitibi-Grenville teleseismic experiment, *J. Geophys. Res.*, *105*, 13,735–13,755.

Sigloch, K. (2011), Mantle provinces under North America from multifrequency *P* wave tomography, *Geochem. Geophys. Geosyst.*, *12*, Q02W08, doi:10.1029/2010GC003421.

Simons, F., A. Zielhuis, and R. van der Hilst (1999), The deep structure of the Australian continent from surface wave tomography, *Lithos*, *48*, 17–43.

Sleep, N. (1990), Monteregian hotspot track: A long-lived mantle plume, *J. Geophys. Res.*, *95*, 21,983–21,990.

Sleep, N. (1997), Lateral flow and ponding of starting plume material, *J. Geophys. Res.*, *102*(B5), 10,001–10,012, doi:10.1029/97JB00551.

Sleep, N. (2003), Geodynamic implications of xenolith geotherms, *Geochem. Geophys. Geosyst.*, *4*(9), 1079, doi:10.1029/2003GC000511.

Sleep, N., C. Ebinger, and J.-M. Kendall (2002), Deflection of mantle plume material by cratonic keels, *Geol. Soc. Spec. Publ.*, *199*, 135–150.

Sol, S., C. Thompson, J.-M. Kendall, D. White, J. VanDecar, and I. Asudeh (2002), Seismic tomographic images of the cratonic upper mantle beneath the Western Superior province of the Canadian Shield: A remnant Archean slab?, *Phys. Earth Planet. Inter.*, *134*, 53–69.

Stern, R. (2005), Evidence from ophiolites, blueschists, and ultrahigh-pressure metamorphic terranes that the modern episode of subduction tectonics began in Neoproterozoic time, *Geology*, *33*(7), 557–560, doi:10.1130/G21365.1.

St.-Onge, M., M. Searle, and N. Wodicka (2006), Trans-Hudson Orogen of North America and Himalaya-Karakoram-Tibetan Orogen of Asia: Structural and thermal characteristics of the lower and upper plates, *Tectonics*, *25*, TC4006, doi:10.1029/2005TC001907.

Thompson, D., G. Helffrich, I. Bastow, J. Kendall, J. Wookey, D. Eaton, and D. Snyder (2011), Implications of a simple mantle transition zone beneath cratonic North America, *Earth Planet. Sci. Lett.*, *312*, 28–36.

Tilmann, F., H. Benz, K. Priestley, and P. Okubo (2001), *P*-wave velocity structure of the uppermost mantle beneath Hawaii from traveltime tomography, *Geophys. J. Int.*, *146*, 594–606.

VanDecar, J., and R. Crosson (1990), Determination of teleseismic relative phase arrival times using multi-channel cross-correlation and least-squares, *Bull. Seismol. Soc. Am.*, *80*, 150–169.

VanDecar, J., D. James, and M. Assumpção (1995), Seismic evidence for a fossil mantle plume beneath South America and implications for plate driving forces, *Nature*, *378*, 25–31.

van der Lee, S., and A. Frederiksen (2005), Surface wave tomography applied to the North American upper mantle, in *Seismic Earth: Array Analysis of Broadband Seismograms*, *Geophys. Monogr. Ser.*, vol. 157, edited by G. Nolet and A. Levander, pp. 67–80, AGU, Washington, D. C.

van der Lee, S., K. Regenauer-Lieb, and D. Yuen (2008), The role of water in connecting past and future episodes of subduction, *Earth Planet. Sci. Lett.*, *273*, 15–27, doi:10.1016/j.epsl.2008.04.041.

van Staal, C. (2005), Northern Appalachians, in *Encyclopedia of Geology*, edited by R. Selley, L. Cocks, and I. Plinner, pp. 72–81, Elsevier, Amsterdam.

Wessel, P., and W. Smith (1998), New, improved version of Generic Mapping Tools released, *Eos Trans. AGU*, *79*, 579–579.

White, D., D. Forsyth, I. Asudeh, S. Carr, H. Wu, R. Easton, and R. Mereu (2000), A seismic-based cross-section of the Grenville Orogen in southern Ontario and western Quebec, *Can. J. Earth Sci.*, *37*, 183–192.

Whitmeyer, S., and K. Karlstrom (2007), Tectonic model for the Proterozoic growth of North America, *Geosphere*, *3*, 220–259.